Int. J. Solids Structures Vol. 17, pp. 345–358
Pergamon Press Ltd., 1981. Printed in Great Britain

0020-7683/81/0301-0345/$02.00/0

STRESS INTENSITY FACTORS FOR CRACKED WEDGES

S. F. STONE

Mechanics and Structures Department, School of Engineering and Applied Science, University of California, Los Angeles, CA 90024, U.S.A.

and

R. A. WESTMANN

Mechanics and Structures Department, School of Engineering and Applied Science, University of California, Los Angeles, CA 90024, U.S.A.

(*Received* 31 *January* 1980; *in revised form* 13 *June* 1980)

Abstract—The elasticity solution to the problem of a cracked semi-infinite wedge is presented. The crack emanates from the wedge apex bisecting the wedge angle. Crack surfaces are subjected to a pair of opposing concentrated forces directed either normal or tangential to the crack plane and located an arbitrary distance from the wedge tip. For the case of small wedge angles closed form results are presented for the crack tip stress intensity factors. These results will be useful in calibrating tapered double cantilever beam specimens.

INTRODUCTION

The tapered double cantilever beam (TDCB) is a commonly used test specimen in fracture mechanics. When properly contoured, such a test configuration possesses the property that the strain energy release rate is relatively constant for a range of intermediate crack lengths. This fact permits the ready evaluation of the fracture properties of the material for a homogeneous specimen or measurement of the fracture strength of an adhesive if the specimen is composed of two adherends bonded together.

For short crack lengths the strain energy release rate depends heavily upon the local geometry and crack length. Determination of the fracture characteristics of the specimen for short cracks requires a detailed stress analysis accounting for the important geometrical features. For example, such an analysis must include the effects of the shape of the specimen, the crack length, the point of load application and the type of load applied.

Approximation of the end of the TDCB by a plane, cracked elastic wedge permits an analytical analysis of the problem. It is the purpose of this paper to present the results of such analysis and to study the role of the relevant geometrical parameters.

The geometry considered is a plane semi-infinite wedge of angle $2\theta_0$. The wedge contains a crack emanating from the wedge apex, the plane of the crack bisecting the wedge angle. The material is taken to be homogeneous, isotropic and linear elastic. The two crack faces are subjected to a pair of opposing concentrated forces directed either normal or tangential to the crack surfaces and located an arbitrary distance from the wedge tip. The solution for the stress and displacement fields is obtained using the classical theory of plane elasto-statics.

In [1] Ouchterlony presented, in addition to other results, a solution for the case of a pair of concentrated forces acting at the wedge apex and normal to the crack surfaces. Keer *et al.*[2] considered the problem of a wedge containing a crack bisecting the wedge angle. They formulated their solution for symmetric loading of the wedge and crack faces and presented numerical results for the case of uniform pressure acting upon the wedge and crack surfaces.

It still remains to solve the elasticity problem of a cracked wedge subjected to concentrated forces arbitrarily located on the crack faces. This problem is important in that the solution provides the Green's function leading to solutions for other loading conditions. Furthermore, the anti-symmetric problem resulting from the application of a pair of opposing concentrated tangential forces has not been previously considered.

After stating the mixed boundary value problem the stress and displacement fields are represented by means of Bromwich integrals and the problem reduced to a pair of dual integral

equations. The first technique is similar to that in [3, 4] where elastostatic problems involving interaction between open notches and cracks were considered and yields good numerical results provided $\theta_0 \geq 45°$. To obtain information for smaller values of θ_0, the problem is solved by a Wiener–Hopf technique and the "multiplying factor" method utilized.

Numerical values for the crack tip stress intensity factors are presented for different wedge angles, load locations and types of loading. As an application of these results, a Dugdale model of the yield zone is developed.

PROBLEM STATEMENT AND REDUCTION TO A PAIR OF DUAL INTEGRAL EQUATIONS

The geometry of the problem, Fig. 1, is best described by employing a polar coordinate system r, θ with coordinate origin at the tip of the wedge. The boundaries of the semi-infinite wedge are located on the lines $\theta = \pm\theta_0$, $r \in (0, \infty)$ where $\theta_0 \in (0, \pi]$†. The line $\theta = 0$ bisects the wedge; a crack of length $a = 1$ extends from the wedge tip along the ray $\theta = 0$.

The wedge is composed of a linearly elastic, homogeneous and isotropic material with E, ν denoting the Young's modulus and Poisson's ratio respectively. For purposes of this analysis, let $E = 1$.‡ The polar components of the displacement vector are denoted by u^α, v^α where the superscript will depend upon the loading. In the same way the polar components of the two-dimensional stress field are σ_r^α, σ_θ^α, $\tau_{r\theta}^\alpha$. The theory of plane stress and an Airy stress function are employed.

Two types of wedge loading are considered. The first is the application to the two crack faces of a pair of opposing concentrated forces of magnitude P, the point of application being $r = l$, $l \in [0, 1)$ and the forces normal to the crack surface. The second type of loading is the same as the first except the forces are directed tangentially to the crack face their magnitude being T. These two loading cases correspond to the superscript $\alpha = 1, 2$ respectively.

Due to the type of loading and geometrical symmetry in this problem, only one-half of the wedge $\theta \in (0, \theta_0)$, $r \in (0, \infty)$ need be considered provided appropriate boundary conditions are enforced on the line $\theta = 0$, $r \in (1, \infty)$. A mathematical statement of the boundary conditions on the line $\theta = 0$, $r \in (0, \infty)$ is as follows:

$$\sigma_\theta^1(r, 0+) = -P\delta(r-l) \quad r \in (0, 1) \tag{1a}$$

$\alpha = 1$ (Normal load)

$$v^1(r, 0+) = 0 \quad r \in (1, \infty) \tag{1b}$$

$$\tau_{r\theta}^1(r, 0+) = 0 \quad r \in (0, \infty) \tag{1c}$$

$$\tau_{r\theta}^2(r, 0+) = -T\delta(r-l) \quad r \in (0, 1) \tag{2a}$$

$\alpha = 2$ (Tangential load)

$$u^2(r, 0+) = 0 \quad r \in (1, \infty) \tag{2b}$$

$$\sigma_\theta^2(r, 0+) = 0 \quad r \in (0, \infty) \tag{2c}$$

where $\delta(\ )$ is the Dirac delta function.

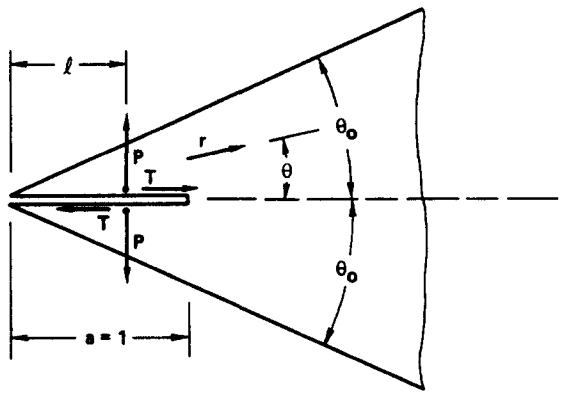

Fig. 1. Geometry of cracked wedge.

†Only values of $\theta_0 \in (0, \pi/2)$ are of interest for the TDCB but a broader range for θ_0 is considered herein.
‡The crack length and elastic modulus are taken to be unity so the problem statement will be in dimensionless form.

The two bounding edges of the wedge $\theta = \pm\theta_0$ are traction free leading to the side conditions

$$\sigma_\theta^\alpha(r, \theta_0) = \tau_{r\theta}^\alpha(r, \theta_0) = 0 \quad r \in (0, \infty) \quad \alpha = 1, 2. \tag{3}$$

Also regularity conditions as $r \to 0$ and $r \to \infty$ require that

$$\sigma_r^\alpha, \sigma_\theta^\alpha, \tau_{r\theta}^\alpha = 0(r^{-\gamma}) \quad \gamma < 1, l \neq 0; \quad r \to 0 \quad \alpha = 1, 2 \tag{4a}$$

$$\sigma_r^\alpha, \sigma_\theta^\alpha, \tau_{r\theta}^\alpha = 0(r^{-\beta}) \quad \beta > 1; \quad r \to \infty \quad \alpha = 1, 2. \tag{4b}$$

Use of the Airy stress function and Mellin transform[3] leads to the following integral representation of the stress and displacement fields

$$r\sigma_r^\alpha(r, \theta) = \frac{1}{2\pi i}\int_{Br}\left\{\frac{d^2}{d\theta^2} - (s-1)\right\}\psi^\alpha r^{-s}\, ds \tag{5a}$$

$$r\sigma_\theta^\alpha(r, \theta) = \frac{1}{2\pi i}\int_{Br} s(s-1)\psi^\alpha r^{-s}\, ds \tag{5b}$$

$$r\tau_{r\theta}^\alpha(r, \theta) = \frac{1}{2\pi i}\int_{Br} s\frac{d}{d\theta}\psi^\alpha r^{-s}\, ds \tag{5c}$$

$$u^\alpha(r, \theta) = \frac{1}{2\pi i}\int_{Br}\left\{\frac{d^2}{d\theta^2} + (s-1)(1+\nu s)\right\}\psi^\alpha \frac{r^{-s}}{s}\, ds \tag{6a}$$

$$v^\alpha(r, \theta) = \frac{1}{2\pi i}\int_{Br}\left\{\frac{d^3}{d\theta^3} + [(2+\nu)s^2 - (1-\nu)s + 1]\frac{d}{d\theta}\right\}\psi^\alpha \frac{r^{-s}}{s(s+1)}\, ds \tag{6b}$$

where

$$\psi^\alpha = A^\alpha \cos[(s-1)(\theta-\theta_0)] + B^\alpha \sin[(s-1)(\theta-\theta_0)] + C^\alpha \cos[(s+1)(\theta-\theta_0)] + D^\alpha \sin[(s+1)(\theta-\theta_0)]. \tag{7}$$

Further, enforcement of the regularity conditions (4a, b) requires that the Bromwich path lie in the strip

$$\mathrm{Re}(s) \in (0, 1). \tag{8}$$

Satisfying boundary conditions (1c), (2c) and (3) permits the expression of $A^\alpha - D^\alpha$ in terms of unknown functions $\Phi^\alpha(s)$ $\alpha = 1, 2$ as follows:

$$A^1 = -C^1 = \frac{-(s+1)\sin(s\theta_0)\sin(\theta_0)\Phi^1}{2\Delta_1} \tag{9a}$$

$$B^1 = \frac{1+s}{1-s}D^1 = \frac{(1+s)}{(1-s)}\frac{[s\sin(\theta_0)\cos(s\theta_0) + \sin(s\theta_0)\cos(\theta_0)]\Phi^1}{2\Delta_1} \tag{9b}$$

$$A^2 = -C^2 = \frac{[s\cos(s\theta_0)\sin(\theta_0) - \sin(s\theta_0)\cos(\theta_0)]\Phi^2}{2\Delta_2} \tag{9c}$$

$$B^2 = \frac{(1+s)}{(1-s)}D^2 = \frac{-(s+1)\sin(s\theta_0)\sin(\theta_0)\Phi^2}{2\Delta_2} \tag{9d}$$

where

$$\Delta_1 = \sin(2s\theta_0) + s\sin(2\theta_0),$$

$$\Delta_2 = \sin(2s\theta_0) - s\sin(2\theta_0).$$

Boundary conditions (1a, b) and (2a, b) remain to be satisfied and for $\alpha = 1$ lead to

$$\sigma_\theta^1(r,0+) = \frac{1}{2\pi i}\int_{Br} s\,\frac{[\sin^2(s\theta_0) - s^2\sin^2(\theta_0)]}{\Delta_1}\Phi^1(s)r^{-s-1}\,ds = -P\delta(r-l) \quad r\in(0,1) \tag{10a}$$

$$v^1(r,0) = \frac{1}{2\pi i}\int_{Br}\Phi^1(s)r^{-s}\,ds = 0 \quad r\in(1,\infty) \tag{10b}$$

while for $\alpha = 2$

$$\tau_{r\theta}^2(r,0+) = \frac{1}{2\pi i}\int_{Br} s\,\frac{[\sin^2(s\theta_0) - s^2\sin^2(\theta_0)]}{\Delta_2}\Phi^2(s)r^{-s-1}\,ds = -T\delta(r-l) \quad r\in(0,1) \tag{11a}$$

$$u^2(r,0) = \frac{1}{2\pi i}\int_{Br}\Phi^2(s)r^{-s}\,ds = 0 \quad r\in(1,\infty). \tag{11b}$$

The final form of the dual integral equations is attained by integrating eqns (10a) and (11a) with respect to r between the limits of 0 and r. For convenience the results are expressed in matrix form as follows:

$$\frac{1}{2\pi i}\int_{Br}[N^{\alpha\beta}]\{\Phi^\beta(s)\}r^{-s}\,ds = \begin{Bmatrix} P \\ T \end{Bmatrix}(1 - H(l-r)) \quad r\in(0,1) \tag{12a}$$

$$\frac{1}{2\pi i}\int_{Br}\{\Phi^\alpha(s)\}r^{-s}\,ds = \begin{Bmatrix} 0 \\ 0 \end{Bmatrix} \quad r\in(1,\infty) \tag{12b}$$

where

$$[N^{\alpha\beta}] = (\sin^2(s\theta_0) - s^2\sin^2(\theta_0))\begin{bmatrix} \frac{1}{\Delta_1} & 0 \\ 0 & \frac{1}{\Delta_2} \end{bmatrix} \qquad \{\Phi^\alpha(s)\} = \begin{Bmatrix} \Phi^1(s) \\ \Phi^2(s) \end{Bmatrix}$$

and $H(x)$ is the Heaviside step function. Equations (12a) and (b) represent two sets of uncoupled dual integral equations since $N^{\alpha\beta}$ is diagonal. Statement in this form permits the solution of both problems at the same time.

FIRST SOLUTION OF THE DUAL INTEGRAL EQUATIONS

The first solution of the dual integral equations parallels the treatment in [3–5] so it is only necessary to outline the steps. First eqn (12a) is rewritten as follows:

$$\frac{1}{2\pi i}\int_{Br}\frac{\tan(\pi s)}{2}\{\Phi^\alpha(s)\}r^{-s}\,ds = \begin{Bmatrix} P \\ T \end{Bmatrix}(1 - H(l-r)) + \frac{1}{2\pi i}\int_{Br}[M^{\alpha\beta}]\{\Phi^\beta\}(s)r^{-s}\,ds \quad r\in(0,1)$$

where

$$[M^{\alpha\beta}] = \frac{\tan(\pi s)}{2}\begin{bmatrix} 1 & 0 \\ 0 & 1 \end{bmatrix} - [N^{\alpha\beta}]. \tag{13}$$

Note that $M^{\alpha\beta}$ vanishes when $\theta_0 = \pi$.

The substitution

$$\{\Phi^\alpha(s)\} = B\left(\frac{1}{2}, s\right)\int_0^1\{\phi^\alpha(t)\}t^{s-(1/2)}\,dt \tag{14}$$

satisfies eqn (12b) and eqn (13) assumes the form

$$\int_0^r \{\phi^\alpha(t)\}\frac{dt}{\sqrt{(r-t)}} = 2(1-H(l-r))\begin{Bmatrix}P\\T\end{Bmatrix} + \frac{1}{2\pi i}\int_{Br} 2[M^{\alpha\beta}(s)]\{\Phi^\beta(s)\}r^{-s}\,ds \quad r\in(0,1). \tag{15}$$

If the presence of $\phi^\beta(s)$ in the r.h.s. of eqn (15) is momentarily ignored then this equation may be viewed as an Abel integral equation for the auxiliary function $\phi^\alpha(t)$.

Inverting this Abel equation and completing details similar to those in[3, 4] permits the reduction of eqn (15) to a Fredholm integral equation of the second kind

$$\{\Omega^\alpha(t)\} = H(t-l)\sqrt{\left(\frac{t}{t-l}\right)}\begin{Bmatrix}1\\1\end{Bmatrix} + \int_0^1 [L^{\alpha\beta}(\xi/t,\theta_0)]\{\Omega^\beta(\xi)\}\frac{d\xi}{\xi} \quad t\in(0,1) \tag{16}$$

where

$$\{\Omega^\alpha(t)\} = \frac{\pi\sqrt{t}}{2}\begin{Bmatrix}\frac{1}{P}\phi^1(t)\\ \frac{1}{T}\phi^2(t)\end{Bmatrix}$$

and

$$[L^{\alpha\beta}] = \frac{1}{2\pi i}\int_{Br}\frac{2[M^{\alpha\beta}]}{\tan(\pi s)}(\xi/t)^s\,ds. \tag{17}$$

The numerical solution of eqn (16) is complicated by the unbounded and discontinuous forcing function. To overcome this difficulty a new variable $\Lambda^\alpha(t)$ is defined

$$\Lambda^\alpha(t) = \Omega^\alpha(t) - H(t-l)\sqrt{\left(\frac{t}{t-l}\right)} \tag{18}$$

and eqn (16) reduces to

$$\{\Lambda^\alpha(t)\} = \int_l^1 \frac{L^{\alpha\alpha}(\xi/t,\theta_0)\,d\xi}{\sqrt{\xi}\sqrt{(\xi-l)}}\begin{Bmatrix}1\\1\end{Bmatrix} + \int_0^1 [L^{\alpha\beta}(\xi/t,\theta_0)]\{\Lambda^\beta(\xi)\}\frac{d\xi}{\xi}$$
$$t\in(0,1),\ \text{no sum on } \alpha. \tag{19}$$

The kernel function $L^{\alpha\beta}$ can be determined by converting the Bromwich integral in eqn (17) to a real line integral which is then evaluated numerically.

Evaluation of the tractions in the crack plane is of particular interest, especially in the neighborhood of the crack tip. As in [3, 4] it is readily shown that

$$\sigma_\theta^1(r,0+) = \frac{P}{\pi}\frac{\Omega_1(1)}{\sqrt{(r-1)}} + 0(1) \quad r\to 1+ \tag{20a}$$

$$\tau_{r\theta}^2(r,0+) = \frac{T}{\pi}\frac{\Omega_2(1)}{\sqrt{(r-1)}} + 0(1) \quad r\to 1+. \tag{20b}$$

The standard definition of the crack tip stress intensity factors K_I, K_{II} is given by

$$\sigma_\theta^1(r,0) = \frac{K_I}{\sqrt{[2\pi(r-1)]}} + 0(1) \quad r\to 1+ \tag{21a}$$

$$\tau_{r\theta}^2(r,0) = \frac{K_{II}}{\sqrt{[2\pi(r-1)]}} + 0(1) \quad r\to 1+ \tag{21b}$$

and knowledge of K_I, K_{II} completely describes the stress field in the neighborhood of the crack tip. Substituting from eqn (18) into (20) and using (21a) and (b) yields the following expressions for the crack tip stress intensity factors

$$K_I = P\sqrt{\left(\frac{2}{\pi}\right)}\left(\Lambda^1(1)+\sqrt{\left(\frac{1}{1-l}\right)}\right) \tag{22a}$$

$$K_{II} = T\sqrt{\left(\frac{2}{\pi}\right)}\left(\Lambda^2(1)+\sqrt{\left(\frac{1}{1-l}\right)}\right). \tag{22b}$$

To recover the role of crack length a in eqns (22), replace P, T by $P/\sqrt{a}$, $T/\sqrt{a}$ and l by l/a.

SOLUTION BY THE WIENER-HOPF METHOD

An alternate approach is required to achieve accurate solutions of eqns (10) or (11) for small values of θ_0. In [6] Williams used the multiplying factor method to solve a similar type of problem and it is convenient to employ the method here. As the details are similar to those presented in [6] only the essential steps are outlined.

Equations (10) and (11) may be restated as follows:

$$\frac{1}{2\pi i}\int_{Br} s[N^{\alpha\beta}]\{\Phi^\beta(s)\}r^{-s-1}\,ds = -\begin{Bmatrix}P\\T\end{Bmatrix}\delta(r-l) \quad r\in(0,1) \tag{23a}$$

$$\frac{1}{2\pi i}\int_{Br}\{\Phi^\alpha(s)\}r^{-s}\,ds = \begin{Bmatrix}0\\0\end{Bmatrix} \quad r\in(1,\infty). \tag{23b}$$

Following the Wiener–Hopf procedure, the kernel functions must be factorized. For example

$$sN^{11} = \frac{\theta_0 s^2}{2\pi}\frac{\Gamma\left(\frac{1}{2}+\frac{s\theta_0}{\pi}\right)\Gamma\left(\frac{1}{2}-\frac{s\theta_0}{\pi}\right)}{\Gamma\left(1+\frac{s\theta_0}{\pi}\right)\Gamma\left(1-\frac{s\theta_0}{\pi}\right)}L_+(s)L_-(s) \tag{24}$$

where

$$L_+(s) = \exp\left\{\frac{1}{2\pi i}\int_{ic-\infty}^{ic+\infty}\frac{\log\left(\frac{1-\xi^2\sin^2(\theta_0)\,\mathrm{cosech}^2(\xi\theta_0)}{1+\xi^2\sin(2\theta_0)\,\mathrm{cosech}(2\xi\theta_0)}\right)d\xi}{\xi-is}\right\} \tag{25}$$

and

$$c\in(-\epsilon,\epsilon) \quad \epsilon\ll 1.$$

The function $L_+(s)$ is regular and non-zero for $\mathrm{Re}(s)>-\epsilon$ while $\lim_{|s|\to\infty} L_+(s)=1$. Furthermore $L_-(s)$ is given by $L_-(s)=L_+(-s)$ and is regular and non-zero for $\mathrm{Re}(s)<\epsilon$. The factorization of sN^{22} is identical to eqn (24) except that eqn (25) must be altered by replacing the term $1+\xi^2\sin(2\theta_0)\,\mathrm{cosech}(2\xi\theta_0)$ by $1-\xi^2\sin(2\theta_0)\,\mathrm{cosech}(2\xi\theta_0)$.

Now define a function $G(\xi)$ by

$$G(\xi) = \frac{1}{2\pi i}\int_{Br}\frac{\Gamma\left(1+\frac{\theta_0}{\pi}(1-s)\right)\xi^{-s}\,ds}{\Gamma\left(\frac{1}{2}+\frac{\theta_0}{\pi}(1-s)\right)L_-(s-1)(s-1)} \tag{26}$$

and note that $G(\xi)=0$ for $\xi\in(0,1)$. Applying the Mellin Transform to both sides of (26) and

replacing s by $s+1$ gives the result

$$\int_1^\infty G(\xi)\xi^s \, d\xi = \frac{\Gamma\left(1-\frac{s\theta_0}{\pi}\right)}{\Gamma\left(\frac{1}{2}-\frac{s\theta_0}{\pi}\right) L_-(s)s}. \tag{27}$$

As suggested by the multiplying factor method, multiply both sides of (23a) by r, replace r by r/ξ, multiply both sides of (23a) by $G(\xi)$ and integrate between the limits of 0, ∞. Upon using (27), eqn (23a) reduces to

$$\begin{aligned}\frac{1}{2\pi i}\int_{Br}\frac{\theta_0 s}{2\pi}\frac{\Gamma\left(\frac{1}{2}+\frac{s\theta_0}{\pi}\right)}{\Gamma\left(1+\frac{s\theta_0}{\pi}\right)} L_+(s)\Phi^1(s)r^{-s}\,ds &= -Pr\int_0^\infty \frac{1}{\xi}G(\xi)\delta\left(\frac{r}{\xi}-l\right)d\xi \\ &= -P\frac{r}{l}G\left(\frac{r}{l}\right)\end{aligned} \tag{28}$$

and a similar expression for $\Phi^2(s)$ upon redefining $L_+(s)$ and replacing P by T.

Note from eqn (23b) that $\Phi^\alpha(s)$ is analytic for $\mathrm{Re}(s) > 0$ while $\Gamma[\frac{1}{2}+(s\theta_0/\pi)]$ only has poles for $\mathrm{Re}(s) \le -(\pi/2\theta_0)$. Accordingly the l.h.s. of (28) vanishes for $r \in (1, \infty)$. Taking the Mellin transform of both sides of (28) then gives the solution

$$\Phi^1(s) = \frac{-2\pi\Gamma\left(1+\frac{s\theta_0}{\pi}\right)}{\theta_0 s\Gamma\left(\frac{1}{2}+\frac{s\theta_0}{\pi}\right) L_+(s)} P\int_0^1 \frac{r}{l}G\left(\frac{r}{l}\right) r^{s-1}\,dr \tag{29}$$

with a similar expression for $\Phi^2(s)$.

It is now straightforward to obtain the asymptotic expressions for the stress $\sigma_\theta(r,0)$, $\tau_{r\theta}(r,0)$ as $r \to 1+$. From eqns (10a), (11a), (21) and (29) it results that

$$K_I = -P\sqrt{\left(\frac{2\pi}{\theta_0}\right)}\frac{1}{l}G\left(\frac{1}{l}\right) \tag{30a}$$

$$K_{II} = -T\sqrt{\left(\frac{2\pi}{\theta_0}\right)}\frac{1}{l}G\left(\frac{1}{l}\right) \tag{30b}$$

where the expression for $L_-(s)$ appropriate for the loading case is used in (26) when evaluating $G(1/l)$.

As a special case, note that if $\theta_0 = \pi$, then $L_+(s) = 1$ and

$$-\frac{1}{l}G\left(\frac{1}{l}\right) = \frac{1}{\sqrt{[\pi(1-l)]}} \quad (\theta_0 = \pi)$$

thereby recovering the classical results. Furthermore, from eqn (26) it can be shown that

$$-\frac{1}{l}G\left(\frac{1}{l}\right) \sim \frac{\sqrt{\theta_0}}{\pi}\sqrt{\left(\frac{l}{1-l}\right)} \quad l \to 1- \tag{31}$$

given asymptotic expressions for K_I, K_{II} as $l \to 1$-for $\theta_0 \in (0, \pi]$.

It remains to evaluate $(1/l)G(1/l)$ for more general values of the geometrical parameters. To accomplish this it is convenient to shift the Bromwich path and recast the line integral into the following form

$$-\frac{1}{l}G\left(\frac{1}{l}\right) = -\frac{1}{2\pi i}\int_{Br'}\frac{\theta_0}{2\pi}\frac{\Gamma\left(\frac{1}{2}+\frac{z\theta_0}{\pi}\right)}{\Gamma\left(1+\frac{z\theta_0}{\pi}\right)}\left\{\frac{\sin(2z\theta_0)+z\sin(2\theta_0)}{\sin^2(z\theta_0)-z^2\sin^2(\theta_0)}\right\} L_+(z)l^z\,dz \tag{32}$$

where $\mathrm{Re}(z) \in (-1, 0)$. Equation (32) is only valid for the case of normal loading, $\alpha = 1$. For tangential loading, $\alpha = 2$, replace the term $\sin(2z\theta_0) + z\sin(2\theta_0)$ by $\sin(2z\theta_0) - z\sin(2\theta_0)$ and alter the definition of $L_+(z)$.

The integral in eqn (32) is readily evaluated by closing the contour in the right plane and summing the residues. All of the poles are simple and located at the zeros of $1/z[\sin^2(z\theta_0) - z^2\sin^2(\theta_0)] = 0$.

Provided $\theta_0 < 146.3°$ the only real zeros are at $z = 0$ and 1. Accordingly, for $\theta_0 < 146.3°$ and the case of normal loading

$$-\frac{1}{l}G\left(\frac{1}{l}\right) = \frac{\theta_0}{2\pi}\left\{\sqrt{\pi}\left(\frac{2\theta_0 + \sin(2\theta_0)}{\theta_0^2 - \sin^2(\theta_0)}\right)L_+(0) - \frac{\Gamma\left(\frac{1}{2} + \frac{\theta_0}{\pi}\right)2\cos(\theta_0)L_+(1)l}{\Gamma\left(1 + \frac{\theta_0}{\pi}\right)(\sin(\theta_0) - \theta_0\cos(\theta_0))}\right\}$$

$$+ \sum_{n=1}^{\infty}\frac{\theta_0}{\pi}\mathrm{Re}\left\{\frac{\Gamma\left(\frac{1}{2} + \frac{\alpha_n\theta_0}{\pi}\right)}{\Gamma\left(1 + \frac{\alpha_n\theta_0}{\pi}\right)}\left(\frac{\sin(2\alpha_n\theta_0) + \alpha_n\sin(2\theta_0)}{\theta_0\sin(2\alpha_n\theta_0) - 2\alpha_n\sin^2(\theta_0)}\right)L_+(\alpha_n)l^{\alpha_n}\right\} \tag{33}$$

where $\alpha_n = \beta_n + i\gamma_n$ are the complex zeros of $\sin^2(z\theta_0) - z^2\sin^2(\theta_0) = 0$ in the positive quadrant and are tabulated in [7].

It is readily shown for the case of normal loading ($\alpha = 1$) that

$$L_+(0) = (L(0))^{1/2} = \left\{\frac{1 - \frac{\sin^2(\theta_0)}{\theta_0^2}}{1 + \frac{\sin(2\theta_0)}{2\theta_0}}\right\}^{1/2} \tag{34}$$

with a corresponding sign change in the denominator for the case of tangential loading $\alpha = 2$. The term $L_+(\alpha_n)$ is evaluated from eqn (25). Setting $c = 0$ and simplifying the integral in (25) leads to the result

$$L_+(s) = \exp\{I(s, \theta_0)\}$$

where

$$I(s, \theta_0) = \frac{s\theta_0}{\pi}\int_0^{\infty}\frac{\log[h(\xi, \theta_0)]\,d\xi}{\xi^2 + (s\theta_0)^2}$$

and

$$h(\xi, \theta_0) = \frac{1 - \frac{\sin^2(\theta_0)\xi^2}{\theta_0^2\sinh^2(\xi)}}{1 + \frac{\sin(2\theta_0)\xi}{\theta_0\sinh(2\xi)}}$$

for the normal loading case, $\alpha = 1$. For the tangential load case, $\alpha = 2$, the $(+)$ sign in the denominator for $h(\xi, \theta_0)$ becomes a $(-)$ sign.

Substituting from eqns (33), (34) into (30) gives the following expressions for the intensity factors

$$\frac{K_I}{P} = \sqrt{\left(\frac{2\theta_0 + \sin(2\theta_0)}{\theta_0^2 - \sin^2(\theta_0)}\right)} - \sqrt{\left(\frac{\theta_0}{2\pi}\right)}\frac{\Gamma\left(\frac{1}{2} + \frac{\theta_0}{\pi}\right)}{\Gamma\left(1 + \frac{\theta_0}{\pi}\right)}\left(\frac{2\cos(\theta_0)L_+(1)}{\sin(\theta_0) - \theta_0\cos(\theta_0)}\right)l$$

$$+ 0\{l^{\beta_1}\mathrm{Re}(\zeta_1 l^{i\gamma_1})\} \quad l \to 0 \tag{35a}$$

$$\frac{K_{II}}{T} = \sqrt{\left(\frac{2\theta_0 - \sin(2\theta_0)}{\theta_0^2 - \sin^2(\theta_0)}\right)} + 0\{l^{\beta_1}\mathrm{Re}(\zeta_2 l^{i\gamma_1})\} \quad l \to 0 \tag{35b}$$

where ζ_1, ζ_2 are complex constants. Note that in the case of tangential loading, the residue at $z = 0$ vanishes so the linear term does not appear in eqn (35b). To recover the crack length parameter in eqns (35) replace l by l/a and P, T by $P/\sqrt{a}$, $T/\sqrt{a}$.

NUMERICAL RESULTS AND DISCUSSION

The numerical method used to solve eqn (19) is identical with that described in [3] with appropriate changes to account for the differences in the kernels and Bromwich paths. As in [3] the integration interval [0, 1] in (19) was divided into N equal subintervals. In extreme cases a partition of $N = 40$ was required to achieve an accuracy of 2.5%. Figure 2 presents $\Lambda^a(t)$ showing the convergence for the representative case $\theta_0 = 45°$, $l = 0.2$.

The stress intensity factors are presented in Figs. 3 and 4 for $\theta_0 \geq 45°$ in the case of normal loading and for $\theta_0 \geq 30°$ for tangential loading. For other values of θ_0 it was not economically feasible to achieve the desired numerical accuracy by this method especially for $l/a \leq 0.6$.

In the special case $\theta_0 = 180°$, $\Lambda^a(t) = 0$ as can be seen from (19) and eqns (22) give the classical results. This illustrates how the first solution method is a perturbation about the $\theta_0 = 180°$ limit case and therefore why it is difficult to obtain accurate numerical results for smaller values of θ_0.

Accurate values for the intensity factors for the lower values of θ_0 are readily obtained from eqns (35) in conjunction with the asymptotic expression (31). Equation (35a) is in complete agreement with Ouchterlony's results[1] for the limit case of $l = 0$. The range of applicability of the first and second term residue expansions in (35a) and (b) can be assessed by evaluating the magnitude of the contribution from the next residue.

The values of β_1 are determined from [7] and it results that the next contribution in the series is $0\{l^{4.2/\theta_0} \operatorname{Re}(\zeta_a l^{i\gamma_1})\}$ as $l \to 0+$. As an example, for $\theta_0 = 30°$, $\beta_1 = 8.02$, suggesting that the linear terms in (35a) and (b) give accurate results for a significant range of values of l with this range increasing as θ_0 decreases. This is further supported by comparing results from eqns (35a)

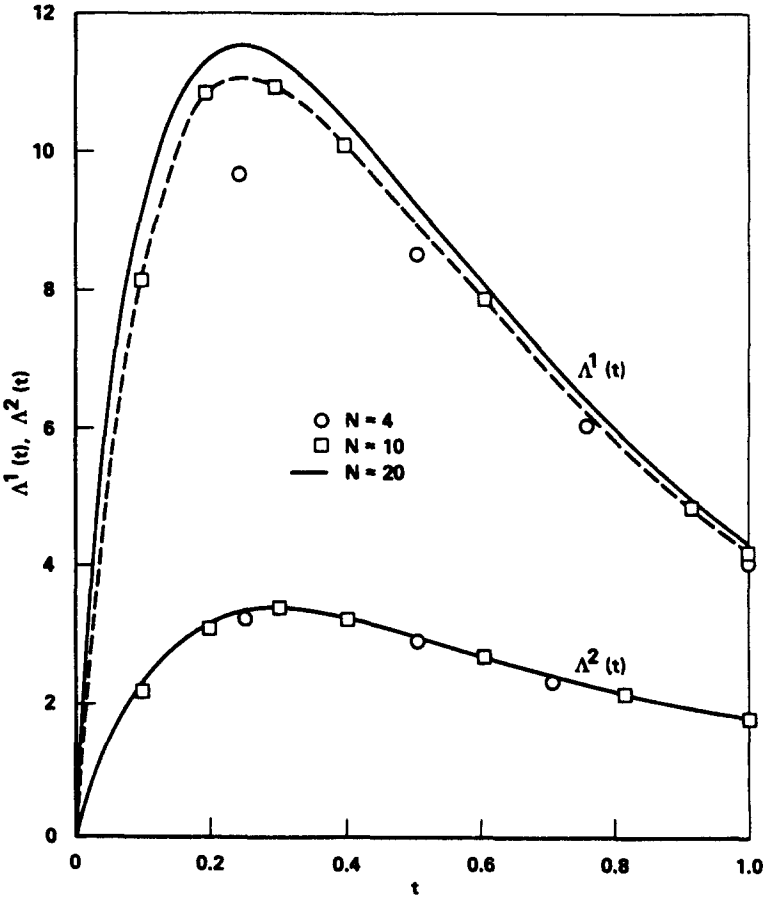

Fig. 2. Solution to integral equation – $\theta_0 = 45°$, $l = 0.2$.

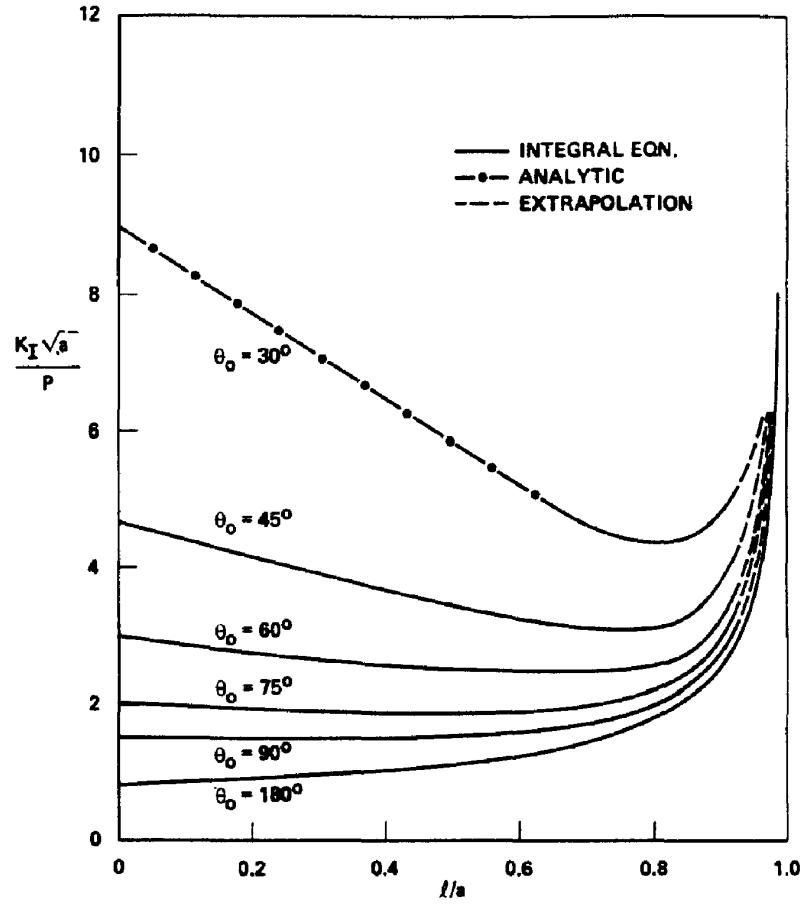

Fig. 3. Stress intensity factor for cracked wedge.

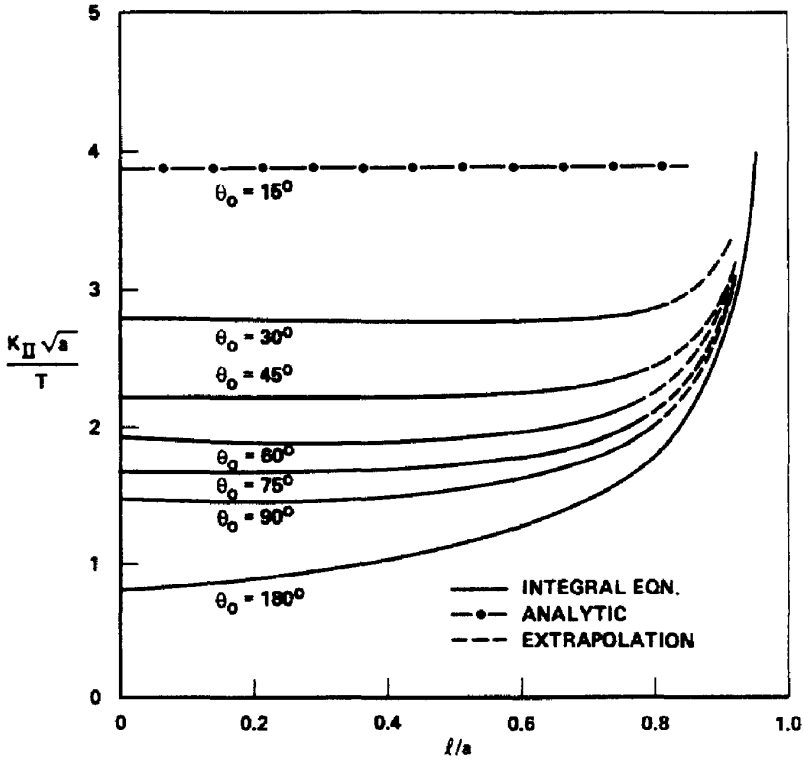

Fig. 4. Stress intensity factor for cracked wedge.

and (b) with the numerical values from (22a) and (b). Figure 3 shows that for $\theta_0 = 45°$ the maximum error is less than 7% provided $(l/a) \leq 0.75$. Similar comparisons in Fig. 4 suggest even better accuracy.

The remainder of this paper is primarily concerned with wedges where θ_0 is small so eqns (35a) and (b) in conjunction with (31) are judged to be sufficiently accurate. The values of $L_+(1)$ have been numerically evaluated and are presented in Fig. 5. An asymptotic expansion for $L_+(1)$ is determined to be

$$L_+(1) = \frac{2}{\sqrt{6}}\theta_0 \quad \text{as } \theta_0 \to 0 \tag{36}$$

and is shown in Fig. 5 as well.

The user of a tapered double cantilever beam specimen is concerned with how the intensity factor depends upon crack length a for a fixed load position l. To see this dependence, reintroduce the crack length into eqn (35a) and normalize the intensity factor by l. Then (35a) assumes the form

$$\frac{K_I\sqrt{l}}{P} = C_0\sqrt{\left(\frac{l}{a}\right)} - C_1\left(\frac{l}{a}\right)^{3/2} \tag{37}$$

where

$$C_0^2 = \frac{2\theta_0 + \sin(2\theta_0)}{\theta_0^2 - \sin^2(\theta_0)}$$

$$C_1 = \sqrt{\left(\frac{\theta_0}{2\pi}\right)}\frac{\Gamma\left(\frac{1}{2}+\frac{\theta_0}{\pi}\right)}{\Gamma\left(1+\frac{\theta_0}{\pi}\right)}\frac{2\cos(\theta_0)L_+(1)}{(\sin(\theta_0) - \theta_0\cos(\theta_0))}$$

The intensity factor $[(K_I\sqrt{l})/P]$ in (37) increases monotonically with a/l for $(a/l) \in [1, 3C_1/C_0)$ and attains its maximum at $(a/l) = (3C_1/C_0)$ where

$$\left(\frac{K_I\sqrt{l}}{P}\right)_{\max} = \frac{2}{3}\sqrt{\left(\frac{C_0^3}{3C_1}\right)}. \tag{38}$$

For values of $(a/l) > (3C_1/C_0)$ the intensity factor decreases monotonically with increasing (a/l) approaching zero like $C_0\sqrt{(l/a)}$ as $(a/l) \to \infty$.

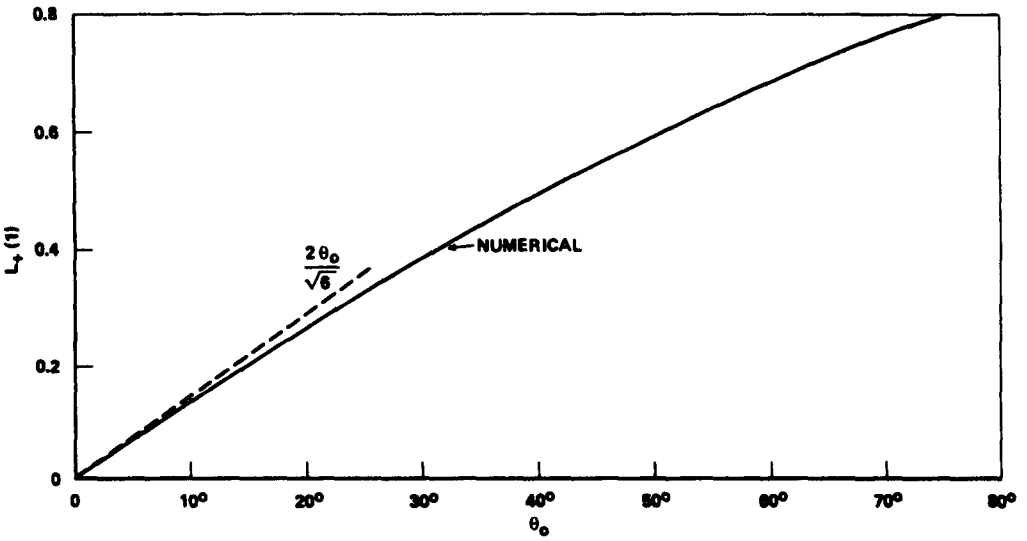

Fig. 5. Dependence of $L_+(1)$ upon θ_0.

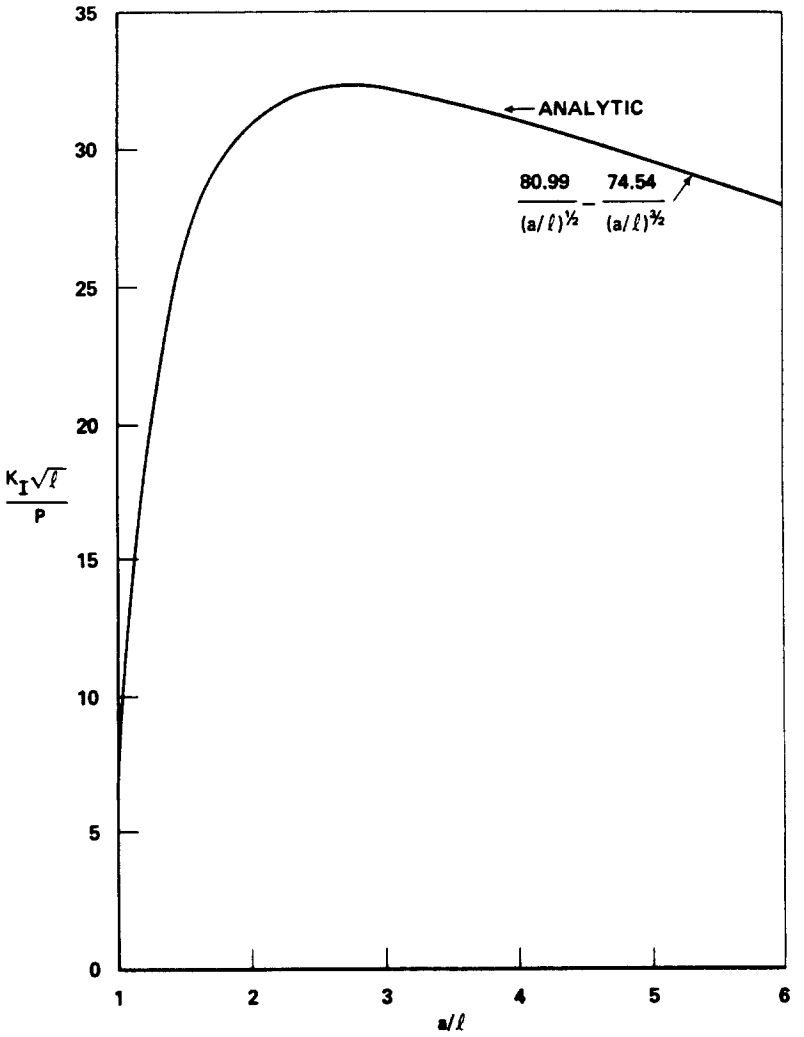

Fig. 6. Dependence of stress intensity factor upon crack length – $\theta_0 = 7°$.

A representative result is presented in Fig. 6 for the case $\theta_0 = 7°$. Equation (37) is valid for at least $(a/l) \geq 1.3$ so the dependence of the intensity factor is captured in virtually closed form for all values of (a/l) of interest. For values of (a/l) close to unity, (37) is not valid and the asymptotic result obtained from (31) should be used

$$\frac{K_I\sqrt{l}}{P} = \sqrt{\left(\frac{2}{\pi}\right)}\frac{l/a}{\sqrt{(1-l/a)}} \quad \text{as} \quad \frac{a}{l} \to 1+. \tag{39}$$

Plotting values from (39) in Fig. 6 is difficult as its region of influence is only $(a/l) \in (1, 1.1]$. Note that for $(a/l) \in [1.8, 4.8]$ the values of $(K_I\sqrt{l}/P)$ range between 30.0 and 32.6. It is these intermediate crack lengths for which K_I is effectively constant and which make the TDCB specimen so useful.

As another application of the results presented herein, consider the calculation of the Dugdale plastic zone size. Consider only normal loads P_0 and denote the point of load application by l_0. Further let the physical crack length be l_1 while the combined length of the crack and Dugdale zone is a. In the Dugdale zone $(r \in (l_1, a), \theta = 0)\sigma_\theta = \sigma_Y$ where σ_Y is the yield stress of the elastic-perfectly plastic material.

The dimensionless curves presented in Fig. 3 may be characterized by

$$\frac{K_I\sqrt{a}}{P} = F\left(\frac{l}{a}, \theta_0\right) \tag{40}$$

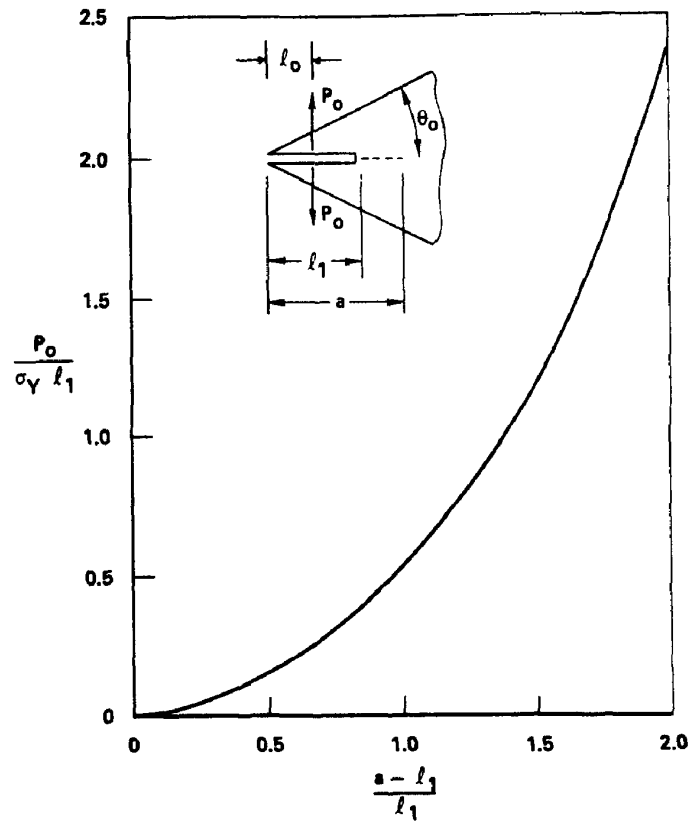

Fig. 7. Load required to create plastic zone $-\theta_0 = 7°$, $(l_0/l_1) = 0.25$.

where for the smaller values of θ_0, $F[(l/a), \theta_0]$ is represented by eqn (35a) and the asymptotic result arising from (31). Now using superposition and eqn (40) the intensity factor at the tip of the Dugdale zone is given by

$$K_I = \sigma_Y \sqrt{a} \left\{ \frac{P_0}{\sigma_Y a} F\left(\frac{l_0}{a}, \theta_0\right) - \int_{l_1/a}^{1} F(\alpha, \theta_0)\, d\alpha \right\}. \tag{41}$$

The intensity factor at the end of the Dugdale zone must vanish giving the following relation

$$\frac{P_0}{\sigma_Y l_1} = \frac{a}{l_1} \frac{1}{F\left[\frac{l_0}{a}, \theta_0\right]} \int_{l_1/a}^{1} F(\alpha, \theta_0)\, d\alpha. \tag{42}$$

The relationship between P_0 and a is readily determined now by substituting a range of values of a into the r.h.s. of (42) and calculating the corresponding values of P_0. The results of such a calculation are shown in Fig. 7 for the special case of $\theta_0 = 7°$, $(l_0/l_1) = 0.25$.

In summary, this paper presents the results of an elastic stress analysis of a cracked wedge subjected to concentrated normal and tangential loads applied to the crack faces. Results for the crack tip stress intensity factors are developed and closed formed expressions given which are valid for a range of values of θ_0, a/l. These closed form results are of great practical value as they permit the accurate calibration of tapered double cantilever specimens.

Acknowledgements—The initial phases of this research were supported by NSF Grant ENG 74-18641. The final phase of this work was completed while one author (Westmann) was on sabbatical leave from UCLA and serving as a Visiting Professor at the California Institute of Technology.

REFERENCES

1. F. Ouchterlony, Symmetric cracking of a wedge by concentrated loads. *Int. J. Engng Sci.* 15, 109–116 (1977).
2. L. M. Keer, D. A. Mendelsohn and J. D. Achenbach, Crack at the apex of a loaded notch. *Int. J. Solids Structures* 13, 615–623 (1977).

3. R. A. Westmann, Geometrical effects in adhesive joints. *Int. J. Engng Sci.* **13**, 369–392 (1975).
4. R. Muki and R. A. Westmann, Crack emanating from an open notch. *J. Elasticity* **4**, 173–186 (1974).
5. R. P. Srivastav and K. S. Parihar, Dual and triple integral equations involving inverse mellin transforms. *SIAM-J. Appl. Math.* **16**, 126–133 (1968).
6. W. E. Williams, A star-shaped crack deformed by an arbitrary internal pressure. *Int. J. Engng Sci.* **9**, 705–712 (1971).
7. L. Ricci, Tavola di radici di basso modulo di un' equazione interessante la scienza delle construzioni. *Rivisita Di Ingegneria* 150–156 (Feb. 1951).